Extended JT-60U Plasma Regimes toward High Integrated Performance

Y, Kamada and the JT-60 Team[1]

Japan Atomic Energy Research Institute, Naka Fusion Research Establishment,
Naka-machi, Naka-gun, Ibaraki-ken, Japan
e-mail contact of main author: kamada@naka.jaeri.go.jp

Abstract

With the main aim of providing physics basis for ITER and the steady-state tokamak reactor, JT-60U has been optimizing operational concepts and extending discharge regimes toward simultaneous sustainment of high confinement, high β_N, high bootstrap fraction, full noninductive current drive and efficient heat and particle exhaust utilizing variety of heating, current drive, torque input and particle control capabilities. In the two advanced operation regimes, the reversed magnetic shear (RS) and the weak magnetic shear (high- β_p) ELMy H modes characterized by both internal (ITB) and edge transport barriers and high bootstrap current fractions f_{BS}, discharges have been sustained near the steady-state current profile solutions under full noninductive current drive with proper driven current profiles (High- β_p; HH_{y2}~1.4 and β_N~2.5 with N-NB, RS; HH_{y2}~2.2 and β_N ~2 with f_{BS}~80%). Multiple pellet injection has extended the density region with high confinement. These operational modes have been extended to the reactor relevant regime with small values of collisionality and normalized gyroradius and $T_e \sim T_i$. In the RS regime, Q_{DT}^{eq}=0.5 has been sustained for 0.8s. Stability has been improved in these regimes by suppression of the neoclassical tearing mode with local ECCD and enhanced β_N-values with wall stabilization. The ITB structure has been controlled by toroidal rotation profile modification and transport studies have revealed a semi-global nature of the ITB structure. The both-leg divertor pumping has enhanced He exhaust by ~40%. Ar-puff experiments have improved confinement at high density with detached divertor due to high pedestal temperature T_i-ped. In H-modes, the core confinement degraded with decreasing T_i-ped suggesting stiff core profiles. The operational region of grassy ELMs with small divertor heat load has been established at high triangularity, high q_{95} and high β_p. The record value of the neutral beam current drive efficiency of 1.55x10 ^{19}A/m^2/W has been demonstrated by N-NB. Abrupt large amplitude events causing neutron drop have been discovered with frequency inside the TAE gap. Disruption studies have clarified that runaway current is terminated by MHD fluctuations when the surface q becomes 2~3.

1. Introduction

The JT-60U tokamak project has addressed major physics and technological issues in the ITER R&D and in developing commercially attractive steady-state reactor concepts such as SSTR. These experimental and demo reactors require simultaneous sustainment of high confinement, high β_N, high bootstrap fraction, full noninductive current drive and efficient heat and particle exhaust. In addition to providing physics basis for each individual element, recent JT-60U research has been directed at the optimization of the operational concepts toward achievement of the high integrated performance, its sustainment in long pulses and extension to the reactor relevant parameter regimes [1-3]. The present paper reviews progress in the JT-60U program after the 17th IAEA Fusion Energy Conference.

2. Improved Heating, Current Drive and Particle Control Capabilities

In order to enhance the integrated performance mentioned above, the profile control is essentially important. Among the world tokamaks, JT-60U has now the largest variety of heating and current drive systems which consist of the conventional positive-ion-based neutral beams (P-NBs; co- and counter-tangential and perpendicular), high energy tangential negative-ion-based NBs (N-NBs) (see Fig.1a)), LHRF, ICRF and ECRF systems. This set of actuators enables ion and electron heating, and central and off-axis heating. Furthermore, the profiles of heating, momentum input and current drive can be controlled independently.

The 110GHz ECRF system [4], initially installed in 1999, now consists of three gyrotrons and has achieved torus input of 1.5MW x3s. This system, designed to couple the fundamental O-mode, launches the ECRF wave from the low field side with an oblique toroidal angle for

1 See Appendix.

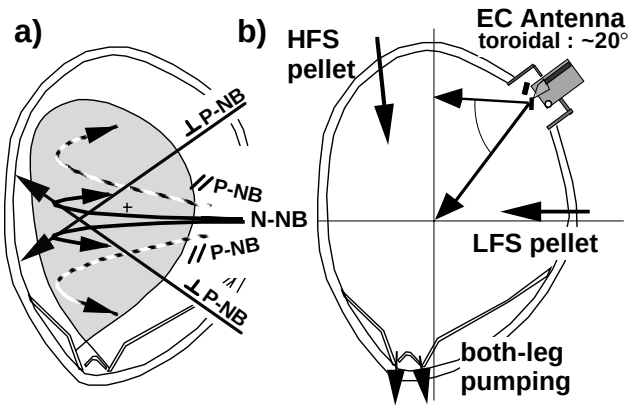

FIG.1 a) Typical high triangularity shape and neutral beam lines, b) newly installed plasma control systems;ECH/CD, pellet injection and both-leg divertor pumping.

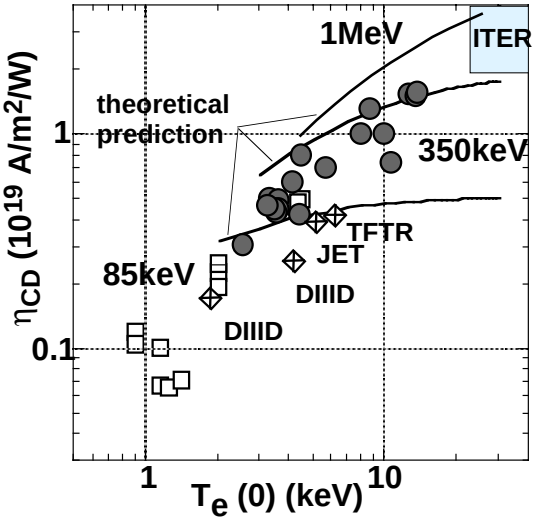

FIG.2 N-NB current drive efficiency (η_{CD}) approaching the ITER regime.

current drive, and the ray can be steered over a range of minor radii by tilting the launching mirror (Fig.1b)). This scheme is the same as the one adopted in ITER. Capability of on- and off-axis heating and current profile control with a typical width of 10cm has been demonstrated [4]. In case of central heating and current drive, strongly peaked profiles of electron temperature T_e have been achieved with $T_e(0)$ up to 15keV and the measured driven current by the MSE system has reached ~0.2MA at $T_e(0)$~6keV and $n_e(0)$~0.7×10^{19}m^{-3}. The measured driven current is consistent with the theoretical calculation with a code using the adjoint equation for the relativistic Fokker-Planck equation [5].

Current drive capability of the N-NB system in JT-60U [6] has been extended to the reactor relevant regime (Fig.2) [7]. In the high temperature regime with $T_e(0)$~10keV, driven current profiles and current drive efficiency η_{cd} evaluated experimentally agree reasonably with theoretical predictions. The N-NB driven current reached 1MA with injection power of 3.75MW at beam energy of 360KeV. The record value of neutral beam current drive efficiency of 1.55×10^{19}A/m^2/W has been obtained in high β_p ELMy H-mode discharges with $T_e(0)$~13keV (see Sec.3).

The outer pumping slot in the W-shaped divertor opened in 1999 permits both-leg-pumping (Fig.1b)) [8]. In early 2000, the new multiple pellet injector was installed. This system injects 2.1mm cubic deuterium pellets with repetition rate of <10Hz and injection speed of 100 - 300m/s for high-field-side (HFS) and 100- 1000m/s for low-field-side (LFS) injection (Fig.1b)).

3. Advanced Modes Sustained near the Steady-State Current Profile Solutions

JT-60U has been optimizing the steady-state operation concepts utilizing two high confinement modes characterized by the magnetic shear profiles naturally expected in the steady-state with high bootstrap fractions: One is the high-β_p (weak positive magnetic shear) H-mode [9] and the other is the reversed magnetic shear (RS) H-mode [10]. In these modes, high confinement is sustained by both the Internal Transport Barrier (ITB) and the edge transport barrier. Inside the ITB radius, both ion and electron thermal diffusivities, χ_i and χ_e, are improved in these modes. However the improvement is different in structure: In case of the high-β_p mode, χ_i and χ_e become as small as the ion neoclassical diffusivity χ_i^{neo} near the axis, but their values stay well above χ_i^{neo} at the ITB radius. Therefore the core pressure gradient ∇p produced is moderate. On the other hand, in the RS mode, both χ_i and χ_e can drop sharply down to the level of χ_i^{neo} within a narrow (~10 cm) layer of the ITB, resulting

in strong ∇p. The ITB stays at a radius with weak positive magnetic shear s<1 in the high-β_p mode (the ITB radius also often seems to be trapped at q=2 or 3 surface) and at a radius with s~0 (~ q_{min}) in the RS mode. In such systems, produced ∇p determines the bootstrap current profile hence the magnetic shear profile. Then the magnetic shear profile determines the pressure profile. Plasmas of these advanced modes are thus self-regulating system with strong correlation between the pressure and the current profiles. Therefore, demonstration of the existence of stable steady-state solutions at high-β_N and high-β_p under full noninductive current drive with proper combination of externally driven current and self-driven bootstrap current is the critical issue. This issue is now one of the main research subjects in tokamaks [1-3,9,10,11-15]. From this point of view, we have achieved favorable discharges in both high-β_p H-mode and the RS H-mode.

Figure 3 shows a stable weak magnetic shear (high-β_p) ELMy H-mode discharge E36715 with high confinement enhancement over the ITER H-mode scaling HH_{y2}=1.4 and high β_N= 2.5 under full noninductive current drive achieved for the first time in JT-60U near the steady state current profile solution [7,16]. The noninductive current drive was achieved mainly by on-axis current drive by N-NB (608kA, 40% of I_p), broad current drive by P-NB (255kA,17 %) and off-axis bootstrap current (760kA, 51%) (see Fig.5 a)). In the later phase of the N-NB pulse, the safety factor at the plasma center q(0) stays almost constant suggesting saturation of current profile evolution. In this phase, the fast ion distribution has also reached steady state according to the 3-D Orbit Following Monte Carlo calculations. Since the NB current drive efficiency increases with $T_e(0)$ [7], on-axis ECH was applied and $T_e(0)$ reached 13keV, and then the record N-NB η_{CD} of 1.55×10^{19} A/m^2/W was achieved. This N-NB injection phase was free from any significant MHD instability (such as sawteeth, m/n=1/1 modes, neoclassical tearing modes etc.) except for type-I ELMs. Figure 3 b) shows the integrated performance of this discharge, which consists of 7 axes: HH_{y2}, β_N, f_{BS} (fraction of bootstrap current to plasma current I_p), f_{CD} (fraction of non-inductive driven current to I_p), fuel purity, ratio of radiated power to absorbed heating power, and line averaged electron density normalized by the Greenwald density limit. The full scale for each axis represents one of the ITER-FEAT steady-state operation design examples. This discharge satisfies the requirements for HH_{y2},f_{BS} and f_{CD}. However, for density and radiation power, in particular,

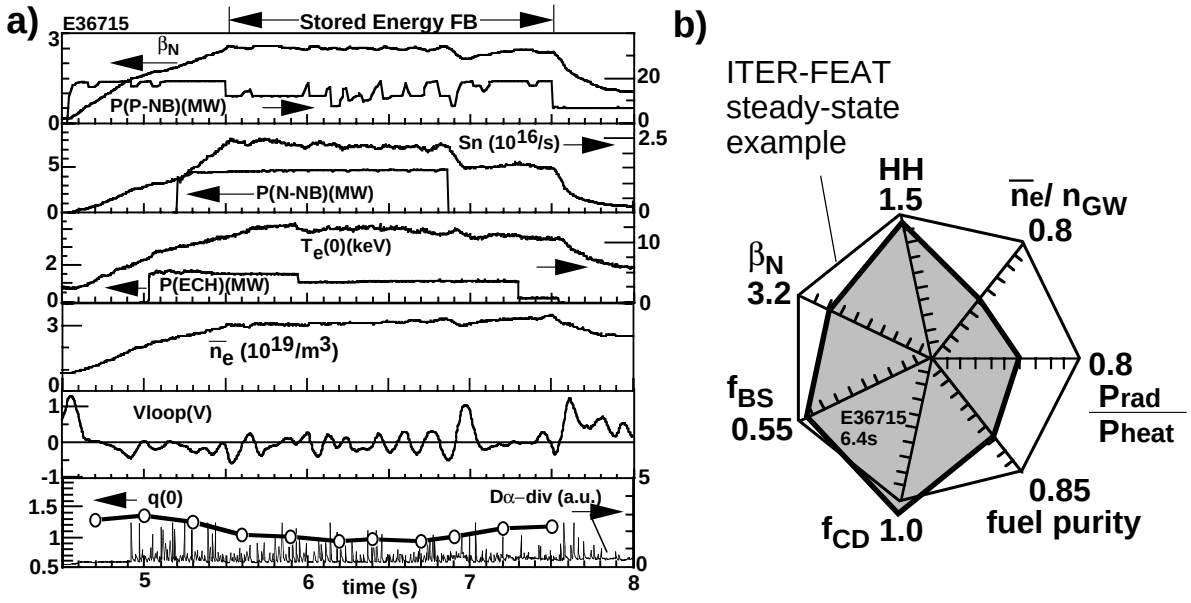

FIG.3 a) Time evolution of the high β_p ELMy H-mode discharge E36715 in which HH_{y2}=1.4 and β_N= 2.5 were sustained under full non-inductive current drive with N-NB (1.5MA, 3.74T,q_{95}=4.75). b) Achieved integrated performance relative to the target values in the ITER-FEAT steady-state operation.

further improvement is needed. For these parameters, an improved integrated performance has been achieved by pellet injection (see Sec.8).

Figure 4 shows a stable RS ELMy H-mode discharge E35037 [17]. We have, for the first time, demonstrated sustainment of the reversed magnetic shear configuration near the steady state solution, self-sustained by a large bootstrap current driven by the steep pressure gradient at the ITB. In this high triangularity (δ =0.43) ELMy RS plasma, β_N~2, HH_{y2}~2.2 and energy confinement enhancement over the ITER89P L-mode scaling H_{89PL}~3.5 were sustained for 2.7 s (6 x energy confinement time τ_E) under full non-inductive current drive with 80% of bootstrap fraction and 25% of P-NB driven current fraction. In this phase, the measured safety factor profiles were almost unchanged (Fig.5c)), because shrinkage of the reversed shear region thus the ITB radius was suppressed by the large bootstrap current peaked at the ITB layer and the current profile was stayed stationary. Figure 4b) shows the integrated performance. In addition to the fairly high values of HH_{y2} and f_{BS}, electron density and radiation fractions are also favorable. The remaining issues in the RS ELMy H-mode are relatively small β_N and insufficient fuel purity. Due to such high confinement performance, in the high current RS plasma E34292 at I_p=2.6MA, the DT equivalent fusion gain Q_{DTeq}=0.5 was sustained for 0.8s (~τ_E) [17]. However, the discharge was terminated by major disruption at low β_N=1.1. The high-β stability is the largest issue for the RS mode.

Figure 5 compares profiles of driven current j , magnetic shear s, safety factor q and ion temperature T_i for a) the weak positive shear case E36715 (Fig.3, full noninductive), b) the flat shear case (partially noninductive), and c) the strong reversed shear case E35037 (Fig.4, full noninductive). Current profiles were controlled by

a) combination of central N-NB and EC current drive (CD) and bootstrap current,

b) ohmic and bootstrap currents without NBCD

c) combination of broad P-NBCD and large bootstrap current.

In all cases, the measured q-profiles or the current profiles in the saturated phase stay near the steady-state solutions calculated by the ACCOME code. By modification of the external current drive profile together with proper combination with bootstrap current, JT-60U has thus sustained high confinement advanced modes near the steady state current profile solutions from the weak positive to the strong reversed shear configurations.

Based on the JT-60U high β_p mode experience, the ITB is formed in the low shear region; typically s<1 [15]. In discharges shown on Figs 5 a) and b), this criterion was held and wide

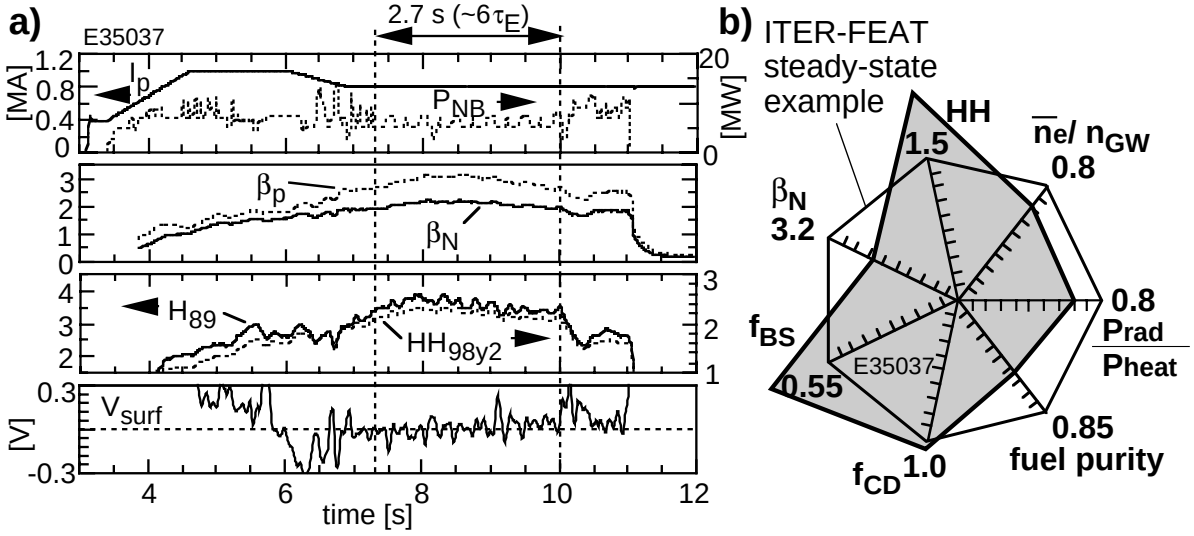

FIG.4 a) Evolution of the Reversed Shear ELMy H-mode discharge E35037 in which HH_{y2}~2.2 and bootstrap fraction ~ 80% were sustained under full non-inductive current drive (0.8MA, 3.4T, q_{95}=9.3). b) Achieved integrated performance relative to the target values in the ITER-FEAT steady-state operation.

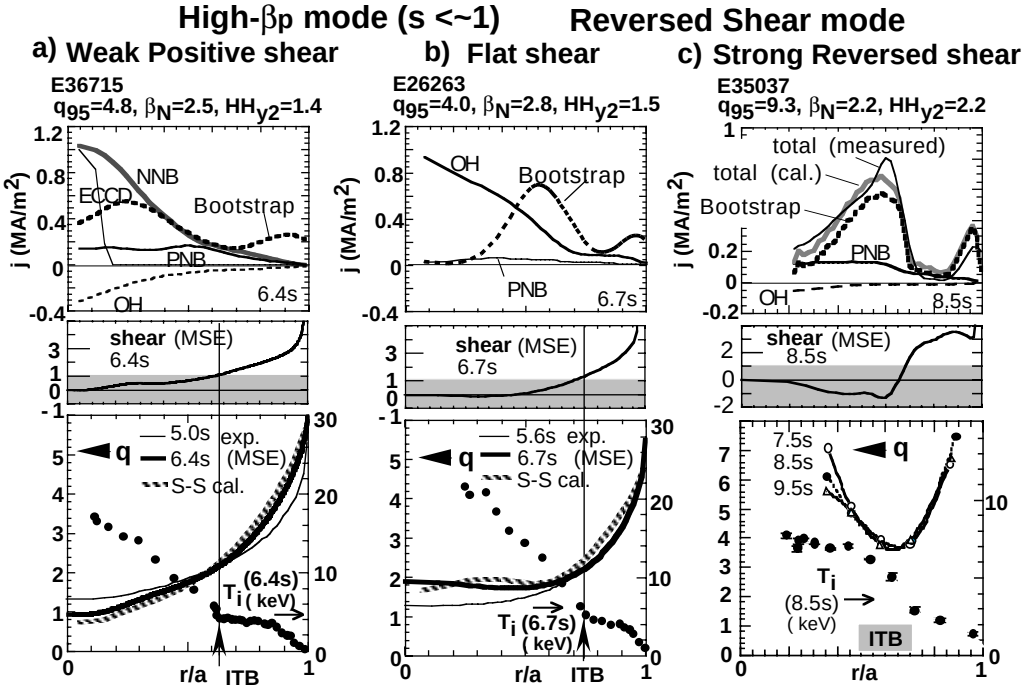

FIG.5 Advanced modes with ITBs sustained near the steady-state current profile solutions by active current drive control: a) the weak positive shear (full noninductive: N-NB central CD + P-NB broad CD + bootstrap; E36715 in FIG.3), b) the flat shear (bootstrap + OH ; not full noninductive), c) the strong reversed shear (full noninductive: P-NB broad CD + high bootstrap fraction; E35037 in FIG .4). a) and b) shows driven current profiles calculated with ACCOME, measured magnetic shear profiles, measured q-profiles in the early phase (thin solid lines), measured q-profiles in the saturated phase (bold solid lines), steady-state q-profiles (ACCOME: S-S cal. ,bold hatched lines) and $T_i(r)$ with ITBs. c) shows similar sets of profiles. The measured current profile is compared with the ACCOME calculation in the top column.

radii satisfying this condition were sustained. As reported in ref.[18], the ITB radius often coincides with the q=2 or 3 surface. The similar result has been also reported from JET [11]. This, however, cannot apply to the conditions of the *initial* formation condition of ITB in JT-60U, which can occur at an inner region where q<2 and s<1, and then the ITB radius expands and is stagnated near the q=2 surface or s~1.

Achieved parameters in the discharges treated in this section are listed in Table I.

4. Extension of the Advanced Mode Regimes

JT-60U has extended the advanced operation regime toward the reactor relevant parameter regimes. Figure 6 a) shows our recent progress toward steady-state improved performance. As a measure describing integrated performance of confinement and stability, we use the product $\beta_N H_{89PL}$. In the high β_p ELMy H-mode regime, $\beta_N H_{89PL}$ ~7 has been sustained for ~1.3s (~3 τ_E) with full noninductive CD and $\beta_N H_{89PL}$ ~5.5 for ~2.8s (~12τ_E) at q_{95}=3.3. In the RS ELMy H-mode regime, $\beta_N H_{89PL}$ ~7.5 has been sustained for ~2.7s (6τ_E) with full noninductive CD. For sustainment of high $\beta_N H_{89PL}$ values, high triangularity operation (δ>0.3 –0.4) is essential. In this paper, triangularity is defined at the separatrix; $\delta = \delta_x$.

Over the past several years, we have increased plasma current and toroidal field in developing high-β_N full noninductive CD plasmas. Figure 6b) demonstrates the significance of this research direction on the ν_e*(collisionality) - ρ_{pi}*(normalized poloidal gyroradius) plane. Since behavior of the key physics processes, such as stability, transport and bootstrap current are determined by these non-dimensional parameters [19], it is necessary to demonstrate the required performances at sufficiently low values of ν_e* and ρ_{pi}* close to the reactor operational regimes. Here, ν_e*= (connection length)/(trapped particle mean free path)

Table I. Achieved Parameters

shot	E34292	E35037	E36715	E37413	E36916
Mode	RS	RS	High-β_p	High-β_p	Ar-puff
	L-mode	ELMyH	ELMyH	ELMyH	ELMyH
	Q_{DT}^{eq}	full-CD	full-CD	Pellet	detached div.
	=0.5 x 0.8s		NNB inj.	NNB inj.	Prad/Pabs=0.76
time (s)	6.7	8.5	6.4	6.95	9.2
I_p (MA)	2.40	0.80	1.5	1.0	1.2
B_t (T)	4.35	3.38	3.74	3.58	2.47
P_{aux}^{abs}(MW)	5.77	5.75	15.3	20.7	12.5
a (m)	0.71	0.78	0.79	0.81	0.84
R (m)	3.09	3.35	3.22	3.37	3.36
δ_x	0.05	0.43	0.36	0.47	0.36
κ_x	1.84	1.56	1.54	1.47	1.40
q_{95}	3.42	9.3	4.75	6.54	3.37
W (MJ)	5.37	2.58	5.98	3.37	2.51
dW_{dia}/dt (MW)	0.66	0.71	0	0	-0.75
S_n (1016/s)	1.18	0.18	2.2	0.86	0.329
Z_{eff}	3.35	3.27	3.06	2.7	4.3
$n_e(0)$ ($10^{19}m^{-3}$)	6.86	3.57	5.0	5.47	4.8
$n_D(0)$ ($10^{19}m^{-3}$)	3.64	1.95	3.0	3.61	2.5
$\overline{n}_e$ ($10^{19}m^{-3}$)	4.04	2.50	3.1	3.39	3.36
$\overline{n}_e/n_{GW}$	0.27	0.61	0.41	0.69	0.65
$T_i(0)$	12.9	7.4	17.5	10.0	9.3
$T_e(0)$	7.3	5.5	12.7	6.5	5.9
τ_E (s)	0.89	0.51	0.39	0.16	0.15
H_{89PL}	2.63	3.74	2.95	1.94	1.50
HH_{y2}	1.44	2.31	1.40	1.05	0.97
β_N	1.12	2.23	2.51	2.22	2.01
β_p	0.75	3.19	1.97	2.40	1.22
β_t(%)	0.87	0.67	1.26	0.77	1.16
f_{BS}	0.45	0.88	0.51	0.59	---
f_{BD}	~ 0	0.25	0.57(NNB 0.40)	0.25	---

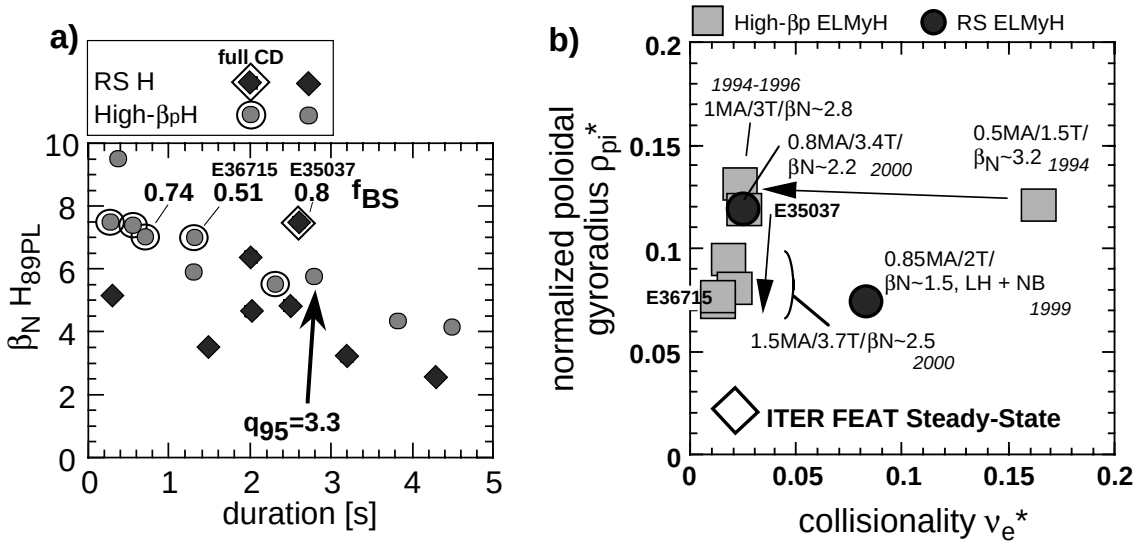

FIG.6 β_N H_{89PL} and sustainment time for reversed shear ELMy H-mode and high-β_p ELMy H-mode discharges (◈ and ◉ : full noninductive CD), b) Operation regime of full noninductive CD at high β_N approaching the ITER regime in terms of normalized poloidal gyroradius ρ_{pi} and collisionality ν_e*.*

~$(n_e qR)/(\varepsilon^{3/2} T_e^2)$, and ρ_{pi}*=(ion poloidal gyroradius)/(minor radius) ~ $T_i^{1/2}/(aB_p)$. In the evaluation of ν_e* and ρ_{pi}*, we used volume average n_e, density weighted volume average T_i and T_e, poloidal field B_p at the edge, q=2, Z_{eff}=1 and ε= 0.5a/R. The JT-60U high-β_N full noninductive CD regime has accessed ν_e*~0.01-0.02 and ρ_{pi}*~0.07-0.1. These values are close to those for the ITER-FEAT steady-state reference design; ν_e*~ ν_e*$_{ITER}$ and ρ_{pi}*~3-4 ρ_{pi}*$_{ITER}$.

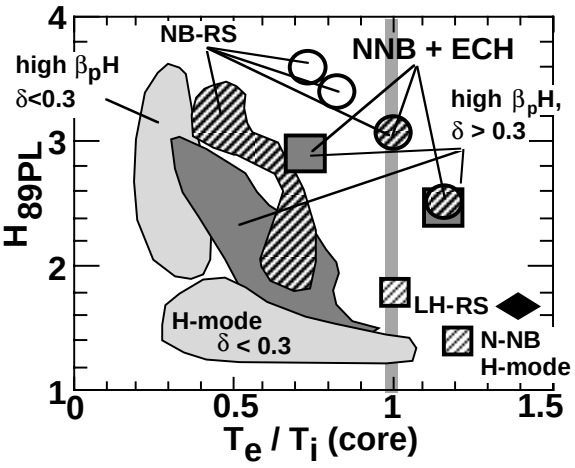

FIG.7 High confinement regime of high-β_p H and Reversed Shear H modes extended to T_e ~ T_i by electron heating (N-NB, EC, LH).

The advanced operation modes in JT-60U were developed originally in the ion heating dominant regime with the 80-90keV NB heating and T_i being much higher than T_e. In order to prove the applicability of these advanced operation modes to fusion reactors, the critical issue is demonstration of high confinement at T_i~T_e. This is because the α-particle heating in reactors is electron heating. In addition, equipartition between ions and electrons is strong in the high density reactor plasmas. For current drive, higher T_e is more beneficial. JT-60U has now favorable capability of electron heating with high energy N-NB, ECRF, LHRF and ICRF minority heating. Figure 7 shows high confinement regimes extended to higher T_e/T_i. In both high β_p ELMy H-mode and RS ELMy H-mode, H_{89PL} =2.5- 3.5 (HH_{y2}~1.2 – 2.2) has been successfully demonstrated at T_e ~T_i.

The remaining issue is achievement of high confinement (H_{89PL}>2.5 or HH_{y2} >1.5) with small central beam fueling. In all high confinement plasmas achieved so far in JT-60U, we injected P-NBs which fuel deuterium to the plasma central region. Although RS plasmas with ITBs have been produced by LH and ECRF with small beam fueling, values of H_{89PL} in these discharges have been less than 2.

Concerning the integrated performance, benefits of the weak shear mode (the high β_p mode), characterized by the relatively moderate ITB, are higher β_N-limit (~2.5 - 3), smaller impurity accumulation (Z_{eff}~2.5-3) and better steadiness at low q_{95} (~3) [9,16]. Benefits of the RS mode, characterized by the strong ITB, are high HH_{y2} (>1.5-2) and high confinement at higher density and at higher T_e/T_i. On the other hand, in the RS mode, the β_N-limit is relatively low (~2) and impurity accumulation is larger (Z_{eff}~3- 3.5) [10]. Since such characteristics are systematically linked to the strength and width of ITBs, development of a control scheme of ITB is crucial. These stability and transport issues are treated in the following two sections.

5. Progress in Understanding and Controlling Stability for the Advanced Modes

Since achievable fusion performance and steadiness of the advanced modes in JT-60U are limited by MHD instabilities [1-3,9,10], identification of these instabilities and development of stabilizing techniques are the most critical issues. In these two years, we have, in particular, concentrated on resistive instabilities and wall stabilization.

In the high β_p ELMy H-mode regime, sustainable β_N-limit has been increased with high triangularity (δ=0.35-0.45) in both low-q (q_{95}~3) and high field regions [9,16] required for ITER R&D. At q_{95}~3.4 (2.1T), β_N=2.6 -3.1 and H_{89PL}~2.2 were sustained for 2.6s even with existence of an m/n=3/2 neoclassical tearing mode with N-NB heating and active feedback control of the stored energy by P-NB heating power modulation. At 3.7T, β_N~2.5 and H_{89PL}

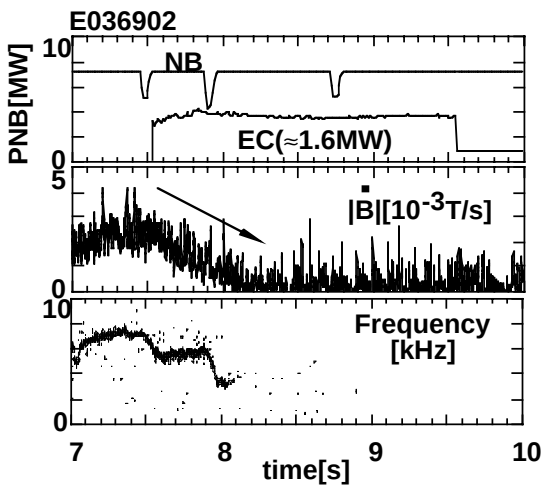

FIG.8 Suppression of the (m/n)=(3/2) neoclassical tearing mode by local ECCD on the mode resonant layer.

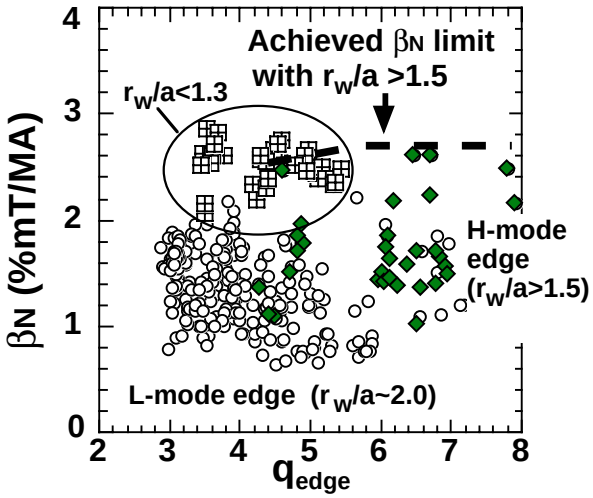

FIG.9 β_N regime of the Reversed Shear discharges increased above the non-wall ideal mode limit by wall stabilization

~2.8 were sustained for 1.3s (E36715, Fig.3) without any significant MHD activity at low values of ν_e* and ρ_{pi}* (see Fig.6 b)).

In the high β_p ELMy H-mode regime, low-n tearing modes ((m,n)=(3,2) or (2,1)) degrade sustainable β_N [9, 16] and enhance fast ion losses[7]. Although the trigger mechanism for the seed island has not been clarified (sawteeth and fishbones are absent), observed parameter dependence suggests that these modes are the neoclassical tearing modes. A simple scaling of the mode onset condition is given by $\beta_N/\rho_{i(toroidal)}^* \sim \nu_e^{*0.36}$ [16]. However, profile effects seem to be equally important. We have clarified experimentally that onset conditions and mode numbers of the tearing mode are determined by local ∇p at the mode rational surfaces. The stable discharge E36715 was sustained with reduction of ∇p at the q=2 surface [16]. In a medium β_N (~1) regime, complete suppression of the neoclassical tearing mode has been demonstrated by local ECCD (1.6MW) applied at the mode resonant surface (Fig.8) [16].

In the RS mode regime, the upper boundary of achievable β_N (~2) is consistent with the ideal low-n kink ballooning limit [10,19]. Whereas, resistive modes appear at lower β_N [20]. Resistive interchange modes with n=1 were found to be destabilized by steep ∇p in the ITB layer (at β_N~1). Higher n (≤3) modes have been observed occasionally at higher β_N. These modes appear as intermittent burst-like activities and do not lead to degradation of global plasma performance by themselves. It is also found that resistive interchange modes located at the inner rational surface can lead to major collapse through a mode coupling with tearing modes destabilized on the outer mode rational surface. Stability analyses with MARG2D [21] revealed that the stability parameter of tearing modes Δ' at the outer mode rational surfaces is affected by free-boundary conditions, supporting experimentally observed high probability of major collapses at the surface safety factors around integer.

In order to improve achievable β_N values by wall stabilization, we have recently tried large bore configurations with (wall radius r_w)/(minor radius a)<1.3 [20]. With this configuration, β_N values were increased by ~10% compared with the no-wall ideal kink ballooning mode limit obtained previously in small bore plasmas (Fig.9). In the wall-stabilized discharges, we observed MHD perturbations which are attributed to the resistive wall mode followed by major disruptions.

6. Internal Transport Barrier Structure and Control

As discussed in Sec.4, development of control schemes of ITB (radial location, width and strength) is the central issue in achieving required integrated performances in particular in

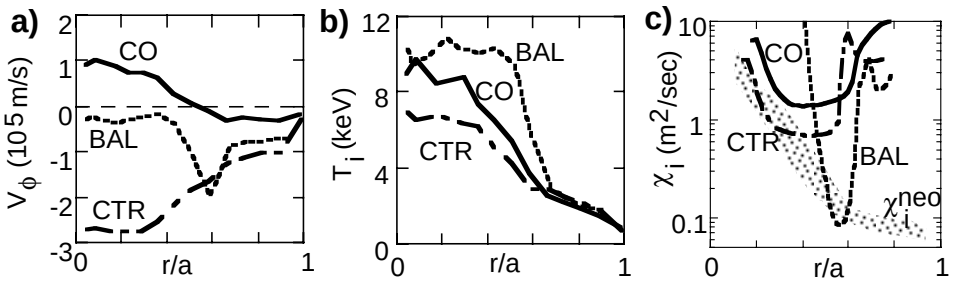

FIG.10 Control of the ITB structure by toroidal rotation profile modification; Co- , Counter- and Balanced injection of the tangential beams (Reversed Shear, I_p=1.5MA, B_t=3.8T, P_{NBinj}=8MW (perpendicular = 4MW + tangential =4MW) .

improving high-β stability and fuel purity. We have demonstrated that the level of diffusivity χ_i in the ITB layer can be changed from 1x to ~10 x χ_i^{neo} by control of magnetic shear profiles from strongly reversed to weakly positive configurations (see sec.3 and [15]). Another method to control the ITB structure is toroidal torque injection [13, 22].

Recently in the strongly reversed magnetic shear regime, active ITB control based on radial electric field shear stabilization has been performed by the toroidal momentum injection in different directions [23]. Figure 10 compares three cases with different toroidal rotation profiles produced by co-tangential NB injection, balanced injection and counter-tangential injection. In the case of the balanced injection, χ_i decreases quickly down to the level of χ_i^{neo} and a steep temperature gradient is produced. Whereas in the cases of co- and counter-injection, the ITB becomes moderate. Figures 11 a) and b) show profiles of radial electric field E_r shear in a discharge where a strong ITB structure initially produced by balanced injection (Fig.11a)) weakened after switching to co-injection. When the ITB started to weaken (Fig.11b)), E_r shear became small only in the outer half region inside the ITB layer due to compensation of the ∇p contribution by the toroidal rotation contribution. (Contribution from the poloidal rotation is small and not plotted for clarity.) After this time, in the whole ITB layer (not only in its outer half region), ion temperature gradient became small. This observation suggests a semi-global structure of the ITB.

Existence of such a semi-global structure has been also observed in research on ITB dynamics [24,25]. Evolution of ITBs in reverse shear and weak positive shear discharges is

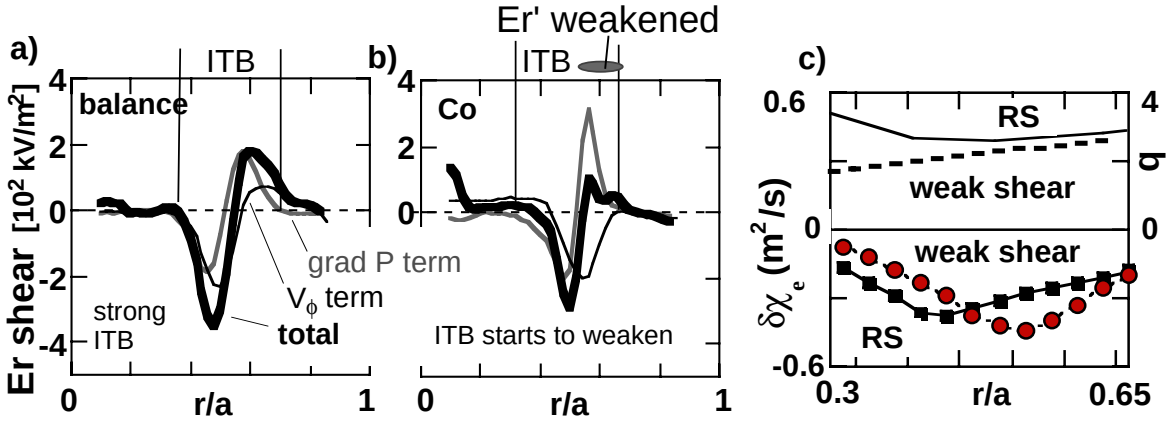

FIG.11 a) and b): E_r profiles in a RS discharge where initial balanced injection was switched to co-injection [23]. a) E_r shear profiles for a strong ITB produced by balanced injection. b) E_r shear profiles when the ITB starts to weaken (after switching to co-injection). E_r shear becomes small only in the outer half ITB layer . c) At the 'ITB event' the diffusivity profile changes ($\delta\chi_e$)abruptly in time and widely in space (~30% of the minor radius) in both weak positive and reversed shear discharges [25]. a) ~ c) suggest a semi global (non-local) dynamics of the ITB structure.

described as a combination of various fast and slow time scales processes. Abrupt in time and specially wide (~0.3 of minor radius) variations of electron and ion heat diffusivities $\delta\chi_{e,i}$, suggesting the semi-global structure, have been found for moderate ITBs in both RS and weak shear plasmas (Fig.11 c)). Such phenomena are called 'ITB event'. The 'ITB event' has been also observed for strong ITBs in RS plasmas. In this case, profiles of $\delta\chi_{e,i}$ is localized near the ITB-foot radius with a narrower width.

7. Progress in Particle Control

For achievement of the required integrated performance (see Figs 3. b) and 4 b)), further improvement is required in fuel purity, in confinement at high density and in high radiation fraction. This section and the next section describe progress in these areas.

The W-shaped divertor of JT-60U was modified from inner-leg pumping to both-leg pumping. After the modification, the pumping rate was improved from 3.2% with inner-leg pumping to 4.6% with both-leg pumping in a divertor-closure configuration, which means both hit points close to the divertor slots. Reduction of carbon impurity and an increase in X-point MARFE onset density have been demonstrated by the forced flow produced by gas puff and effective divertor pumping [8]. The threshold heating power for the L-H transition has been decreased by ~30% compared to the previous open divertor configuration [27].

Efficient helium exhaust has been realized in the divertor-closure configuration with both-leg pumping [8]. The helium exhaust efficiency has been enhanced by 40% with both-leg pumping compared with inner-leg pumping. Global helium particle confinement time of τ^*_{He}= 0.4 s and τ^*_{He}/τ_E = 3 has been achieved in attached ELMy H-mode plasmas. In these ELMy H-mode discharges, τ^*_{He}/τ_E decreases with increasing divertor recycling or, in other words, increasing neutral pressure at the pumping slots. By using central helium fueling with He-beam injection, the helium removal from the core plasma inside ITB in RS plasmas has been investigated for the first time with the divertor-closure configuration [8]. Helium density profiles inside ITB are peaked compared with those in standard ELMy H-mode plasmas. In case of low recycling divertor, it is difficult to achieve required helium exhaust efficiency. However, enhanced helium exhaust efficiency has been achieved in RS plasmas with high recycling divertor.

Multiple pellet injection enabled us to widen particle control capability, in particular control of density profiles and the linkage between electron density and particle recycling. We have found that increase in n_e for the HFS pellet injection is larger than that for the LFS pellet injection in the ELMy H-mode plasmas with heating power of 13 MW. Fueling efficiency for the HFS pellet is independent of the NB heating power, while fueling efficiency for the LFS pellet decreases with increasing the NB heating power.

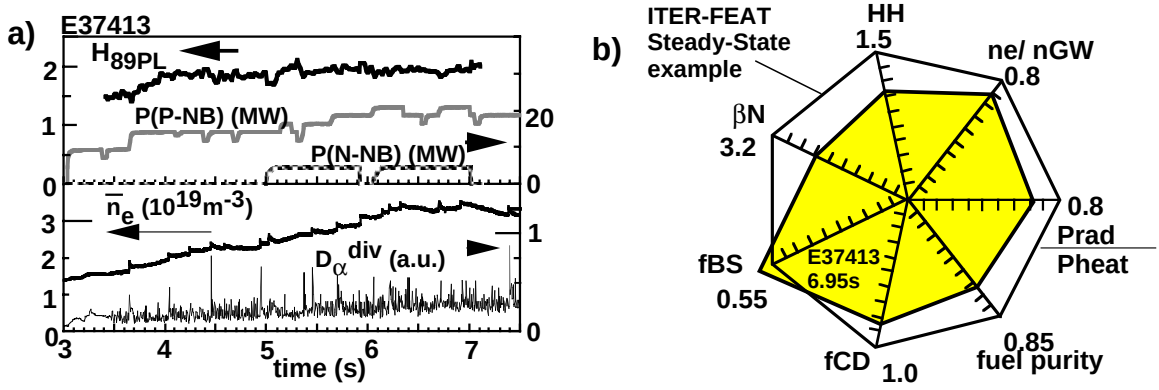

FIG.12 Time evolution and the integrated performance (6.95s) of the pellet fueled High β_p ELMy H-mode discharge with N-NB and P-NB heating (1MA, 3.6T, q_{95}=6.5). At t~7s, $\bar{n}_e/n_{GW}$ reaches 70 %. Achieved values are listed in Table I.

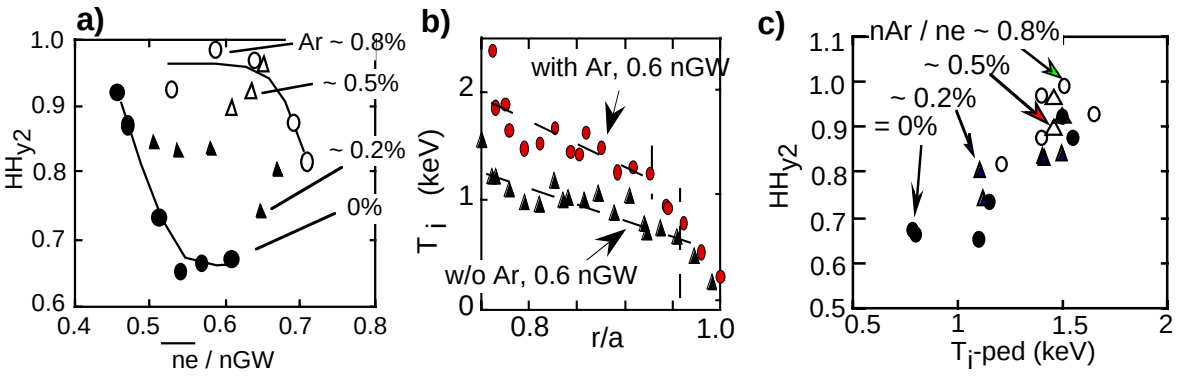

FIG.13 a) Improved confinement in the high density regime with increasing fraction of Ar. (1.2 MA, 2.5T, q_{95}=3.4, δ=0.36) b) T_i at the H-mode pedestal shoulder is higher with Ar puff than without Ar puff at the same $\bar{n}_e$. c) The HH_{y2} factor decreases with decreasing pedestal ion temperature T_i-ped. Over the wide range of Ar-fraction, data points follow the same tendency.

With the HFS pellet injection, JT-60U has successfully extended the density range in the high β_p ELMy H-mode regime. We adopted high triangularity (δ~0.47), since high-δ is beneficial to achieve high confinement at high density (see Sec.8). In addition, we injected N-NBs which can keep a centrally peaked heating profile at high density. Figure 12 a) shows time evolution of one such discharge (E37413: detailed parameters are given in Table I). In this discharge, HH_{y2}=1.05 together with β_N=2.2 and f_{BS}~60% was achieved at $\bar{n}_e/n_{GW}$~0.7. Without pellets, $\bar{n}_e/n_{GW}$~0.6 is the upper density limit to achieve HH_{y2} >1. Compared with Fig.3 b), the integrated performance (Fig.12 b)) was improved in terms of density, radiation power and purity. In this case, the density profile is gradually peaking in time, and the edge temperature stays almost constant even though the edge density is increasing.

8. Extended H-mode Regimes

In order to achieve sufficiently high fusion gain and high radiative power in the SOL and divertor regions, high density operation is essential for tokamak reactors. However energy confinement (the H-factor) in ELMy H-modes tends to degrade with increasing density. Recently energy confinement in the high density region has been remarkably enhanced with Ar injection.

In ELMy H-mode discharges with Ar injection (1.2MA, 2.5T, q_{95}=3.4, δ=0.36), HH_{y2} ~1 has been obtained with a high radiation loss power fraction (~80%) at $\bar{n}_e/n_{GW}$ ~0.65 (Table I) [28]. The HH_{y2}-factor is ~50% higher than that without Ar injection. The main reason for

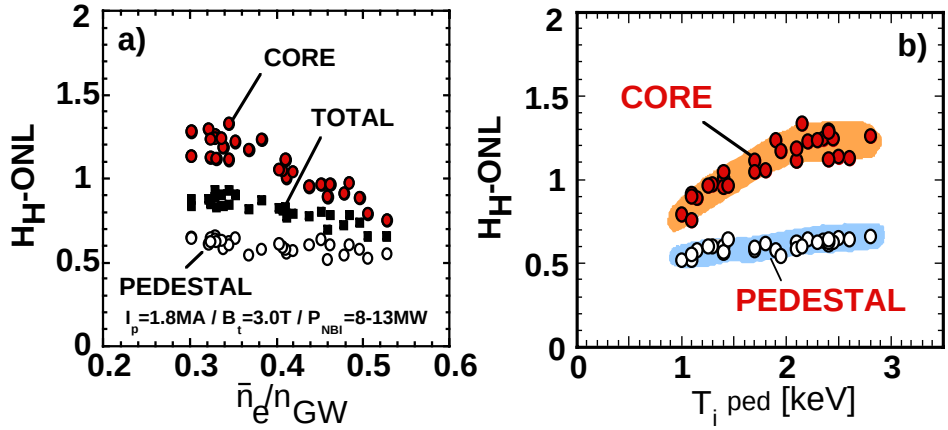

FIG.14 a) Confinement enhancement factors of the core and pedestal components over the offset nonlinear scaling of the ELMy H-mode (deuterium only, 1.8MA, 3.0T, q_{95}=3.0, δ=0.18) . With increasing density, core confinement is degrading while the pedestal confinement stays almost constant. b) The core HH factor decreases with decreasing T_i-ped when T_i-ped<~2keV.

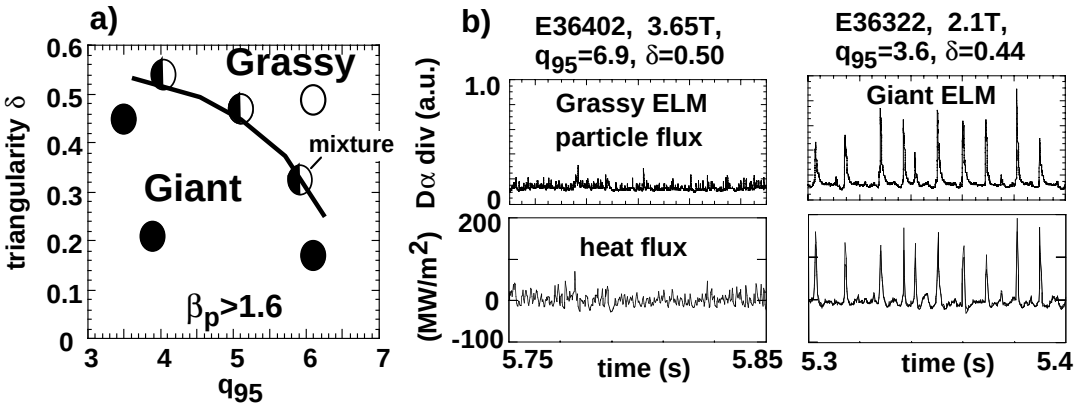

FIG.15 a) Giant ELMs disappear and minute grassy ELMs appear when triangularity >~0.4, q_{95}> ~5 and β_p>~1.6. b) In case of the minute grassy ELMs, both the peak heat load and particle flux on to the divertor plates become much smaller (~1/5) compared with the giant ELMs.

high confinement achieved by Ar injection seems to be higher edge temperature than without Ar at the same density (Fig.13): The HH_{y2} factor increases in the high density regime with increasing fraction of Ar. Ion temperature T_i at the H-mode pedestal shoulder, T_i-ped, is higher with Ar puff than without it at the same n_e. The HH_{y2} factor increases with increasing T_i-ped. Over the wide range of Ar-fraction, data points follow the same tendency.

The relationship between the pedestal temperature and core confinement has been carefully studied for the type I ELMy H-mode plasmas (without Ar) [30]. We have evaluated energy confinement enhancement over the offset non-linear scaling for ELMy H-modes [31]. The scaling consists of two terms: one corresponds to the core part and the other corresponds to the pedestal part. Figure 14 shows confinement improvement factors for both the pedestal and the core parts, and the total enhancement factor. It should be emphasized that the total confinement degradation with increasing density is due to the degradation in the core region and not in the pedestal region. In the type I (Giant) ELMy discharges in JT-60U, the pedestal pressure stays roughly constant (npedTped ~ const.) for fixed I_p, B_t and plasma shape. Therefore, pedestal temperature decreases with increasing pedestal density. As seen in Fig. 14 b), the core enhancement factor decreases with decreasing pedestal temperature when T_i-ped <~2 keV [30,32]. This dependence suggests stiffness of core profiles [32] in the high density H-mode in JT-60U [34].

In our Ar injection experiments, although the Giant (type I) ELM frequency decreased with increasing Ar-fraction, the peak divertor heat load was not changed [36]. In fusion reactors, high confinement should be sustained in H-mode discharges without harmful ELM heat pulses inducing erosion of divertor plates. The grassy ELMy H-mode operation is one of the candidates to satisfy this condition. We have identified the Grassy ELMy discharge region [35]. In JT-60U H-mode plasmas, giant (type I) ELMs disappear and minute grassy ELMs appear when triangularity δ, edge safety factor q_{95} and β_p are high enough: Complete suppression of giant ELMs was observed at δ~0.45, q_{95}~6 and β_p~1.6 (Fig.15 a)). At higher δ (0.54), giant ELMs can disappear at a lower q95 (~4.0). In the grassy ELMy H-mode, peak heat load and particle flux are much smaller than those at Giant ELMs (Fig.15 b)) . The pedestal temperature and pressure, thus the confinement enhancement factor can be higher than those in giant ELMy H-mode without increase in impurity concentration. Edge stability analyses have revealed that the edge plasma is accessing to the second stability regime of high n ballooning mode in grassy ELMy discharges [35,36]. Ideal stability analyses with careful equilibrium reconstruction including edge bootstrap current using EFIT shows possibility of intermediate n (=5 -10) modes as the trigger mechanism of giant ELMs and n> 10 modes as the trigger of grassy ELMs [36].

9. Progress in High Energy Ion Physics

Instabilities with frequency sweeping (FS) in the frequency range of Alfvén eigenmodes have been found during N-NB injection in JT-60U discharges with energetic ion parameters similar to those of α particles expected in ITER: 0.1 % < $<\beta_h>$ < 1 % and $v_{b//}/v_A$ ~1 [37]. One type of the observed instabilities, the slow FS mode, appears with the frequency inside the Alfvén continuum spectrum and its frequency increases to a gap frequency of TAE on the time scale of ~200 ms which is determined by the bulk equilibrium evolution. Another type, the fast FS mode, appears with its frequency in the TAE gap, and the instability bursts last for 1 - 5 ms. Most of the Fast FS modes consist of several branches with fast frequency sweeping of 10-20 kHz in 1 - 5 ms. During the fast FS mode, abrupt large-amplitude events, ALEs, often appear (Fig.16) causing large drop of neutron emission rate and significant increase in fast neutral particle fluxes. Loss of energetic ions increases with increasing amplitude of magnetic fluctuations. Observed energy dependence of the fast ion loss suggests the resonant interaction between energetic ions and the mode.

10. Termination of Runaway Current at Disruption

In order to achieve safe operation at major disruptions, termination of runaway current has been the remaining large issue. In JT-60U, we demonstrated that the runaway current terminates in an early phase of current quench by magnetic fluctuation which appear when surface safety factor q_s decreases to 3 - 2 during the vertical displacement event (Fig.17) [38, 39]. The runaway electron current, observed by hard X-ray emission with energy larger than 1MeV, starts to decrease at q_s~3 coinciding with appearance of n=1 magnetic fluctuations. In all cases, the runaway current terminated at $q_s \geq 2$. Halo current, measured by Rogowski coil installed under the baffle plates, is small during the runaway current termination. It increases after termination of the runaway current and reaches its maximum at q_s~1.

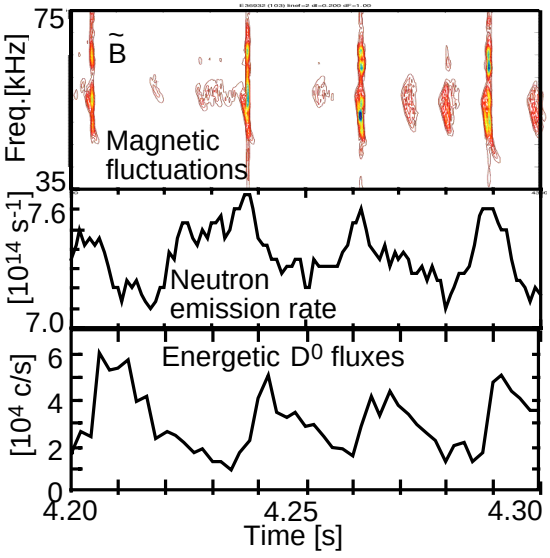

FIG.16 Abrupt large-amplitude events (ALEs) with frequency inside the TAE gap often appear with drop of neutron emission and increase in fast neutral particle flux.

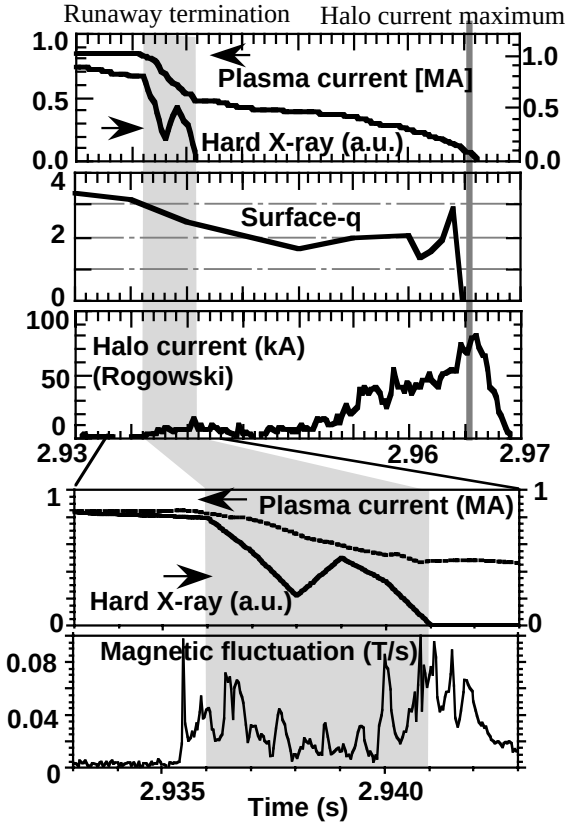

FIG.17 Runaway current at the major disruptions is terminated by n=1 magnetic fluctuation when the surface q becomes low (~2 - 3). Halo current increases after termination of runaway current.

11. Summary

Over the past two years, JT-60U has made a significant progress in establishing physics basis for ITER and steady-state tokamak reactors.

• JT-60U has been optimizing operational concepts and extending discharge regimes toward simultaneous sustainment of high confinement, high β_N, high bootstrap fraction, full noninductive current drive and efficient heat and particle exhaust utilizing variety of heating, current drive, torque input and particle control capabilities including newly installed ECH/ CD, both-leg divertor pumping and pellet injection systems. The record value of neutral beam current drive efficiency $1.55 \times 10^{19} A/m^2/W$ has been demonstrated by N-NB.

• In the two advanced operation modes, reversed shear (RS) and weak shear (high-β_p) ELMy H-modes characterized by both internal and edge transport barriers and high bootstrap current fractions f_{BS}, discharges have been sustained near the steady-state current profile solutions under full noninductive current drive with proper driven current profiles (High β_p; HH_{y2}~1.4 and β_N~2.5 with N-NB, RS; HH_{y2}~2.2 and β_N ~2 with f_{BS}~80%).

• In the high current RS regime, Q_{DT}^{eq}=0.5 has been sustained for 0.8s.

• These operational modes have been approaching the reactor relevant parameter regime in terms of small values of collisionality and normalized gyroradius, and $T_e \sim T_i$. Multiple pellet injection has extended the density region with high confinement.

• Stability has been improved in these modes by suppression of the neoclassical tearing mode with pressure profile optimization and with local ECCD on the mode resonant layer in high-β_p ELMy H mode discharges and by enhanced β_N-values above the no-wall ideal mode limit with wall stabilization in the RS mode discharges. In the RS regime, resistive interchange modes, coupling of the resistive interchange mode and the tearing mode leading to low-β_N collapses, and resistive wall modes have been observed.

• Controllability of the ITB structure has been experimentally confirmed by both current and toroidal rotation profile modifications. Transport studies, including observation of the 'ITB event' have suggested a semi-global nature of the ITB structure.

• The both-leg divertor pumping has enhanced He exhaust by ~40% in ELMy H-mode discharges. Pumping efficiency increases with increasing divertor recycling. Helium density profiles inside ITB are peaked compared with those in standard ELMy H-mode plasmas. In case of low recycling divertor, it is difficult to achieve required helium exhaust efficiency. However, enhanced helium exhaust efficiency has been achieved in RS plasmas with high recycling divertor.

• In the H-mode research, Ar-puff has improved energy confinement by ~50% in the high density regime > $0.6n_{GW}$ with detached divertor due to high pedestal temperature T_i-ped. In ELMy H-modes, the core confinement degrades with decreasing T_i-ped suggesting stiffness of core profiles. The operation region of grassy ELMs with small divertor heat load has been established at high triangularity, high q_{95} and high β_p with the second stable regime access for the high-n ideal ballooning mode. Possible roles of intermediate n ideal modes have been proposed as trigger mechanisms for Giant and Grassy ELMs,

• Abrupt large-amplitude events (ALEs) leading to neutron drop have been discovered with frequencies inside the TAE gap. Observed energy dependence of fast ion loss suggests the resonant interaction between energetic ions and the mode.

• Disruption studies have clarified that runaway current is terminated by MHD fluctuations when the surface q becomes 3 ~ 2.

ACKNOWLEDGMENT

The authors wish to thank continuous effort of engineering and technical staffs in JAERI contributing to the JT-60U project, and scientific contributions under international and domestic collaboration programs.

REFERENCES

[1] Ishida, S. and JT-60 Team, Nucl. Fusion **39** (1999) 1211.
[2] Kamada, Y. and JT-60 Team, Plasma Phys. Control. Fusion **41** (1999) B77.
[3] Ide, S. and JT-60 Team, Phys. Plasmas **7** (2000), 1927.
[4] Ikeda, Y., et al., IAEA-CN-77/EXP4/03, this conference.
[5] Hamamatsu K.,et al., Fusion Technology in press
[6] Grisham, L.R., et al., IAEA-CN-77/FTP1/17, this conference.
[7] Oikawa, T., et al., IAEA-CN-77/EX8/3, this conference.
[8] Sakasai, A., et al., IAEA-CN-77/EX5/5, this conference.
[9] Kamada, Y., *et al., Fusion Energy* (Proc. 16th Int. Conf. , Montreal, 1996), (IAEA Vienna, 1997) Vol.1, p. 247, Kamada, Y., et al., Nucl. Fusion **39** (1999) 1845.
[10] Fujita, T., et al., Nucl. Fusion **39** (1999) 1627.
[11] Soldner, F. X. *et al.*, Nucl. Fusion **39** (1999) 407.
[12] Rice, B. W., *et al.*, Nucl. Fusion **39** (1999) 1855.
[13] Greenfield, C. M. et al., Phys. Plasmas **7** (2000), 1959.
[14] Gruber, O., *et al.* Phys. Rev. Lett. **83**, 1787 (1999)
[15] Kamada Y., Plasma Phys. Control. Fusion **42** (2000) A65.
[16] Isayama, A., et al., IAEA-CN-77/EXP3/03, this conference.
[17] Fujita, T., et al., IAEA-CN-77/EX4/1, this conference.
[18] Koide, Y., et al., Phys. Rev. Lett. **72** (1994) 3662.
[19] Manickam, J., et al., Nucl. Fusion **39** (1999) 1819.
[20] Takeji, S., et al., IAEA-CN-77/EX7/2, this conference.
[21] Tokuda, S., et al., IAEA-CN-77/THP2/10, this conference.
[22] Synakowski, E. J., et al., Nucl. Fusion **39** (1999) 1733.
[23] Sakamoto, Y., IAEA-CN-77/EX6/4, this conference.
[24] Neudatchin, S.V., et al., Plasma Phys. Control. Fusion **41** (1999) L39.
[25] Neudatchin, S.V., et al., IAEA-CN-77/EXP5/01, this conference.
[26] Sakasai, A., et al., J. Nucl. Mater. **266-269** (1999) 312.
[27] Tsuchiya, K., et al., IAEA-CN-77/EXP5/26, this conference.
[28] Kubo, H., et al., IAEA-CN-77/EX5/3, this conference.
[29] Takizuka, T., et al., IAEA-CN-77/THP1/22, this conference.
[30] Urano, H., et al., submitted to Plasma Phys. Control. Fusion
[31] Takizuka, T., et al., Plasma Phys. Control. Fusion 40 (1998) 851.
[32] Janeschitz, G., et al., Proc. 26th EPS Conf. on Control. Fusion and Plasma Phys., Maastricht (Geneva: EPS) vol. **23 J** (1999) 1445.
[33] Hatae, T., et al., IAEA-CN-77/ITERP/03, this conference.
[34] Mikkelsen, D.R., et al., IAEA-CN-77/EXP5/20, this conference.
[35] Kamada Y., et al., Plasma Phys. Control. Fusion **42** (2000) A247.
[36] Lao, L., et al., IAEA-CN-77/EXP3/6, this conference.
[37] Shinohara, K., et al., IAEA-CN-77/EXP2/05, this conference.
[38] Yoshino, R., et al., Nucl. Fusion **40** (2000) 1293.
[39] Tamai, H., et al., IAEA-CN-77/EX9/2, this conference.

Appendix

THE JT-60 TEAM

H.Adachi 1), H.Akasaka, N.Akino, K.Annou, T.Arai, K.Arakawa, N.Asakura, M.Azumi, P.E.Bak 2), M.Bakhtiari 3), C.Z.Cheng 4), S.Chiba, Z.Cui 5), S.A.Dettrick 6), N.Ebihara, G.Y.Fu 4), T.Fujii, T.Fujita, H.Fukuda 1), T.Fukuda, A.Funahashi, H.Furukawa 1), L.R.Grisham 4), K.Hamamatsu, T.Hamano 1), T.Hatae, A.Hattori 1), N.Hayashi, S.Higashijima, S.Hikida 1), K.W.Hill 4), S.Hiranai, H.Hiratsuka, H.M.Hoek 7), A.Honda, M.Honda, Y.Hoshi 1), N.Hosogane, L.Hu 8), H.Ichige, S.Ide, Y.Idomura, K.Igarashi 1), Y.Ikeda, A.Inoue 1), M.Isaka, A.Isayama, N.Isei, S.Ishida, K.Ishii 1), Y.Ishii, T.Ishijima 9), M.Ishikawa 9), A.Ishizawa 10), K.Itami, T.Itoh, T.Iwahashi 1), K.Iwasaki 1), M.Iwase 10), K.Kajiwara 10), E.Kajiyama 1), Y.Kamada, A.Kaminaga, T.Kashiwabara 1), M.Kawai, Y.Kawamata, Y.Kawano, M.Kazawa, H.Kikuchi 1), M.Kikuchi, T.Kimura, Y.Kishimoto, S.Kitamura, A.Kitsunezaki, K.Kizu, K.Kodama, Y.Koide, M.Koiwa 1), S.Kokusen 1), T.Kondoh, S.Konoshima, G.J.Kramer 11), H.Kubo, K.Kurihara, G.Kurita, M.Kuriyama, Y.Kusama, N.Kusanagi 1), L.L.Lao 12), P.Lee 5), S.Lee 10), A.W.Leonard 12), J.Li 8), M.A.Mahadavi 12), J.Manickam 4), K.Masaki, H.Masui 1), T.Matsuda, M.Matsukawa, T.Matsumoto, D.R.Mikkelsen 4), M.Z.Mironov 13), Yukitoshi Miura, Yushi Miura, N.Miya, K.Miyachi, H.Miyata 1), K.Miyata 1), Y.Miyo, T.Miyoshi 10), K.Mogaki, M.Morimoto 1), A.Morioka, S.Moriyama, K.Nagashima1), S.Nagaya, O.Naito, Y.Nakamura, T.Nakano, R.Nazikian 4), M.Nemoto, S.V.Neudatchin 14), Y.Neyatani, H.Ninomiya, T.Nishitani, H.Nobusaka 1), M.Noda 1), T.Oba 1), T.Ohga, K.Ohshima 1), A.Oikawa, T.Oikawa, M.Okabayashi4), T.Okabe, J.Okano, K.Omori, S.Omori, Y.Omori, H.Oohara, T.Oshima, N.Oyama 10), T.Ozeki, T.Petrie 12), G.Rewoldt 4), J.A.Romero 15), N.Sakamoto, A.Sakasai, S.Sakata, T.Sakuma 1), S.Sakurai, T.Sasajima, N.Sasaki 1), M.Sato, M.Seimiya, H.Seki 1), M.Seki, Y.Shibata3), K.Shimada, M.Shimada, K.Shimizu, M.Shimizu, M.Shimono, K.Shinohara, S.Shinozaki, H.Shirai, M.Shitomi, X.Song 8), M.Sueoka, A.Sugawara 1), T.Sugie, H.Sunaoshi, Masaei Suzuki 1), Mitsuhiro Suzuki 1), S.Suzuki 10), T.Suzuki, Y.Suzuki 10), M.Takahashi 1), S.Takahashi 1), S.Takano 1), M.Takechi 10), S.Takeji, H.Takenaga, Y.Taki 1), T.Takizuka, H.Tamai, Y.Tanai 1), T.Terakado, M.Terakado, K.Tobita, S.Tokuda, T.Totsuka, R.Toyokawa 1), K.Tsuchiya, T.Tsuda, T.Tsugita, Y.Tsukahara, K.Uehara, T.Uehara 1), N.Umeda, Y.Uramoto, H.Urano 3), K.Ushigusa, K.Usui, S.Wang 8), J.Yagyu, M.Yamaguchi 1), Y.Yamashita 1), H.Yamazaki 1), K.Yokokura, I.Yonekawa, H.Yoshida, R.Yoshino

1) Staff on loan
2) STA Fellow, Denmark
3) Fellow of Advanced Science
4) PPPL, USA
5) STA Exchange, SWIP, China
6) STA Fellow, Australian Nat.Univ.
7) JAERI Fellow, Sweden
8) STA Exchange, Academia Sinica, China
9) JAERI-Univ.Tsukuba, Cooperative Doctoral Program
10) Post-Doctoral Fellow
11) STA Fellow, Netherlands
12) GA, USA
13) STA Fellow, Ioffe Inst., RF
14) JAERI Fellow, Kurchatov Inst., RF
15) STA Fellow, Spain